Different growth response of mountain rangeland habitats to annual weather fluctuations

Fabio Oriani[a,b,c] ,Helge Aasen[b] , Manuel K. Schneider[a,c]

a
Forage Production and Grassland Systems, Agroscope, Reckenholzstrasse 191, Zurich, 8046, Switzerland
b
Water Protection and Substance Flows, Agroscope, Reckenholzstrasse 191, Zurich, 8046, Switzerland
c
Grazing Systems, Agroscope, Reckenholzstrasse 191, Zurich, 8046, Switzerland

March 13, 2024

Non-peer reviewed preprint submitted to EarthArXiv and Remote Sensing in Ecology and Conservation

Graphical Abstract

Different growth response of mountain rangeland habitats to annual weather fluctuations

Fabio Oriani, Helge Aasen, Manuel K. Schneider

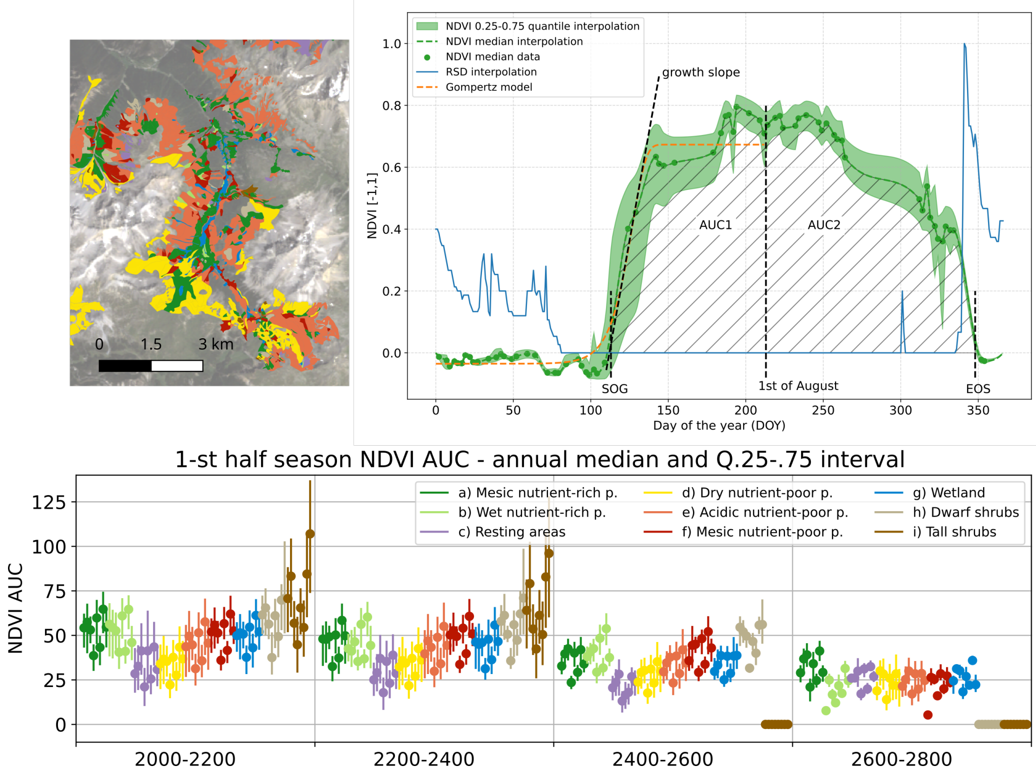

Highlights

Different growth response of mountain rangeland habitats to annual weather fluctuations

Fabio Oriani, Helge Aasen, Manuel K. Schneider

- Satellite monitoring reveals differing growth dynamics in mountain rangelands.
- Dry pasture habitats are more spatially variable and correlated to elevation than wet ones.
- Differences among habitats are reduced at high elevation.
- Late snow melt causes a later but faster growth in pastures.

Different growth response of mountain rangeland habitats to annual weather fluctuations

Fabio Oriani[a,b,c], Helge Aasen[b], Manuel K. Schneider[a,c]

[a] *Forage Production and Grassland Systems, Agroscope, Reckenholzstrasse 191, Zurich, 8046, Switzerland*
[b] *Water Protection and Substance Flows, Agroscope, Reckenholzstrasse 191, Zurich, 8046, Switzerland*
[c] *Grazing Systems, Agroscope, Reckenholzstrasse 191, Zurich, 8046, Switzerland*

Abstract

An accurate long-term monitoring of mountain rangelands is of primary importance for biodiversity conservation and sustainability of pastoral land use. In this study, we investigate how the seasonality of growth in nine habitats composing the alpine rangeland ecosystem responds to differences in weather conditions from year to year and how these changes occur along the elevation profile. We apply a novel pixel-based analysis over an area of 1000 km^2 in mid-to-high elevation pastures surrounding the Swiss National Park (south-eastern Swiss Alps). By means of NDVI, we track the growth of different habitats across the period 2016-2023. The results suggest that wet and mesic pastures tend to grow more than dry units in an elevation range of 2000-2400 m a.s.l, while all habitats present a similar growth above 2400 m. Moreover, while growth in the first season half is strongly controlled by snow persistence, it is in part compensated by very fast growth after late-melting snow. Conversely, in the second half season, the growth pattern is limited by the arrival of snow in autumn, very abruptly in tall shrubs. Inter-annual weather fluctuations impact equally the habitats and more in the first half of

the growth season. This workflow presents as an effective strategy to monitor the seasonal and long-term evolution of mountain rangeland vegetation in the complex alpine domain.

Keywords: mountain pastures, sentinel-2, ndvi, climate change, remote sensing, snow persistence

---

1. Introduction

Mountain rangeland vegetation covers ice- and rock-free zones on mountain ranges above the treeline. Communities of well-adapted cold-climate species have evolved to cope with harsh climatic conditions and shallow soils with limited nutrient availability [1, 2]. In the European Alps, these habitats have been grazed for millennia by domestic and wild ruminants [3]. While change in land management by pastoralism remains the biggest change factor in alpine flora [4, 5, 6], it is also significantly affected by variations in growth conditions [7, 8, 9]. In the alpine domain, the seasonal dynamics and productivity of grassland is affected by changes in temperature, water availability, and snow persistence [10, 11], with variable altitudinal distribution of the species [12, 13]. A comprehensive yet detailed monitoring of the evolution of mountain grassland is therefore of primary importance to correctly manage the pastoral activity, maximise its sustainability, and preserve the biodiversity of these unique environments.

An attractive approach to monitor alpine vegetation is satellite remote sensing, which regularly captures images of remote and extensive alpine areas, difficult to monitor with proximal sensing or ground survey. Because of the tendency of living vegetation to reflect near-infrared more than red light [see e.g. 14], the reflectance spectrum of vegetation can inform about its photosynthetic activity. In particular, the Normalized Difference Vegetation Index (NDVI), obtained from multiband images, and other spectral indices have been used to track grassland composition and state, the seasonal growth [15, 16] and assimilation [17, 18, 19, 20]. Other studies investigate the correlation between NDVI and biomass [21, 22, 23], or its quality [24, 25]. Pasture spatiotemporal variations [26, 27], its coverage, conversion, and degradation in time [28, 29, 30] have also been monitored by means of spectral indices.

In mountain regions, satellite remote sensing can be combined with species-habitat modeling to detect pasture conversion [31, 21] and monitor its management [32, 33]. Predictive classification has been recently developed to detect thematic classes linked to species richness, productivity, or topographic setting [34, 35, 36]. Modeling experiments analyze the pasture productivity and its degradation in relation with drought conditions [37] and to detect invasive species [38, 39]. The mentioned studies efficiently track the regional variability and change in the spatial distribution of the whole grassland environment.

With the present contribution, we advance this research frontier by focusing on the different local habitats composing mountain rangelands in fine-scale patterns. The driving research questions are:

- Whether the analysis of multispectral satellite images can detect differences in the growth season of the single mountain pasture habitats.

- How their seasonality varies in function of elevation and interannual weather variability, in particular snow persistence.

- How the NDVI-based growth pattern can suggest any relation with known growth-dynamics processes in the first and second halves of the growing season.

To answer these questions, we analyze the images provided by the satellite constellation Sentinel-2 over an area of 1000 Km^2 of the Grisons canton (Switzerland), where nine habitats including dry and wet pastures, resting areas, and shrubs are mapped by field observations. Based on the popular spectral index NDVI, the annual variation of the growing season is analysed for each habitat. We derive statistical indicators from the obtained growth curves with the goal of analysing the relative changes in the vegetation growth along the elevation profile. Moreover, we analyse the impact of snow cover on different seasonal growth parameters over a period of eight years (2016-2023). This way, we characterize and compare the growth in these habitats in terms of their dependence on elevation and weather variability.

2. Study region and data

The Region Of Interest (ROI) of the study consists of the rangelands in the surroundings of the Swiss National Park in the Grisons canton, in an area of approximately 1000 km^2 in south-east Switzerland (Figure 1). The region has been ground mapped for the mountain pasture habitats using the methodology of [40]. The mapping involves the delineation of polygons of uniform vegetation larger than 400 m^2. To each polygon, a dominant vegetation type is attributed. In case of small-scale variability, two or three subdominant types are noted. The mountain rangelands cover sparse little portions of the ROI, with a total mapped surface available after preprocessing of 35.7 km^2.

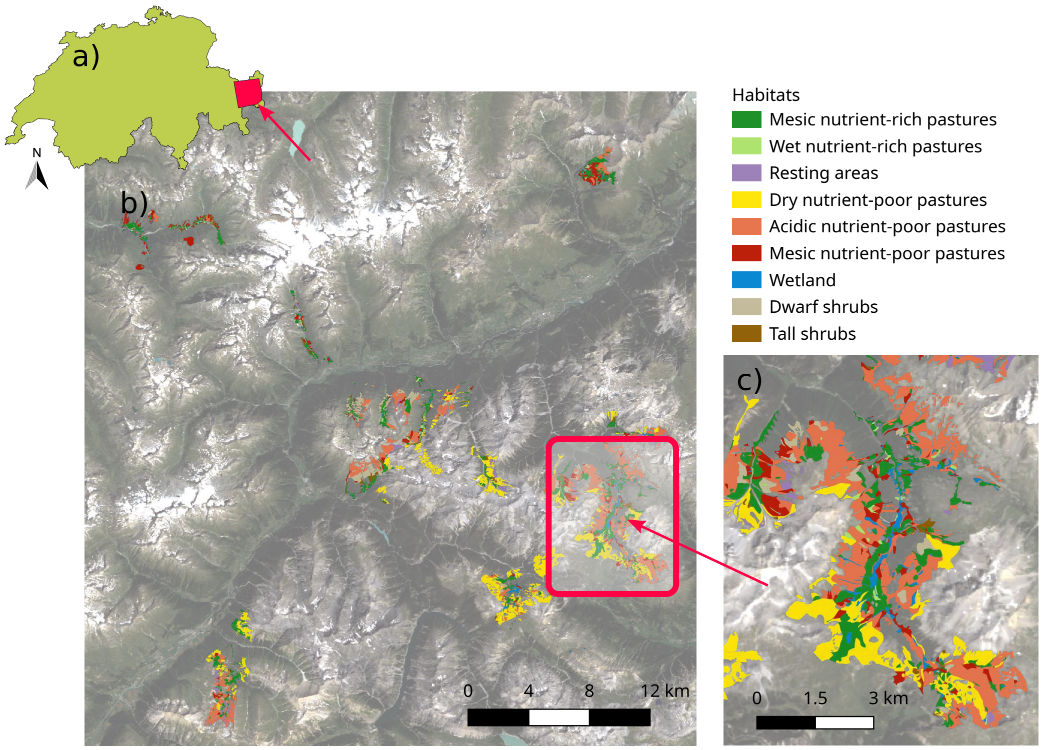

Figure 1: Map of the study area: a) location in Switzerland, b) main map, c) detail showing the habitat units distribution.

The vegetation types were aggregated to nine classes (Table 1) representing the most common rangeland habitats in the region, originating from the combination of pasture management and topographic setting. Those include nutrient-rich pastures (green shades in Figure 1), covering a consistent portion of land along the fluvial axis of the valleys or close to buildings and roads, together with wetlands (blue color), characterised by constantly saturated soils. Distributed in higher altitude mainly above 2000 m (Table 1) are

Table 1: Descriptive table of the habitat units listing their total analyzed surface and the frequency distribution of the elevation values represented by its median ($Q_{0.5}$), the 0.25 ($Q_{0.25}$), and 0.75 ($Q_{0.75}$) quantiles. The surface values refer to south-ward pixels filtered by a prescribed 90-270 degrees aspect range (see section 3.3)

Analyzed surface		Elevation [m]		
Unit Name	[Km^2]	$Q_{0.25}$	$Q_{0.5}$	$Q_{0.75}$
Mesic nutrient-rich pastures	3.31	1769	2110	2283
Wet nutrient-rich pastures	0.19	1997	2150	2411
Resting areas	0.18	2053	2316	2528
Dry nutrient-poor pastures	2.57	2299	2371	2453
Acidic nutrient-poor pastures	5.69	2288	2419	2548
Mesic nutrient-poor pastures	2.25	1836	2159	2311
Wetland	0.51	2055	2163	2263
Dwarf shrubs	0.67	2197	2281	2367
Tall shrubs	0.51	2083	2186	2255

dry, acidic, and mesic nutrient-poor pastures (yellow-to-red colors in Figure 1). They constitute the main part of the land cover, with a drier, thinner, and less fertile soil layer. In addition, high-altitude zones are populated by dwarf and tall shrubs (brown shades in Figure 1), and by sporadic species-poor resting areas (purple color).

2.1. Ancillary variables

To analyse the elevation distribution of the habitats the digital elevation model (DEM) swissAlti3D by Swisstopo (`https://www.swisstopo.admin.ch/en/geodata/height/alti3d.html`) was retrieved for the study region and interpolated to the target grid.

Moreover, to put in relation the annual growth curves with snow persistence, the daily snow depth time series was retrieved from the Scuol station from the Meteoswiss network, lying in the center of the ROI (`https://www.meteoswiss.admin.ch/services-and-publications/applications/measurement-values-and-measuring-networks.html#station=SCU`). To display the annual snow depth time series along with the annual growth curve, the Relative Snow Depth (RDS) is computed by normalizing the values in the range [0,1].

3. Methods

A workflow was developed to analyze the growth pattern of the mountain grassland habitats (for the implementation see the Code Availability section), composed by three main steps: 1) acquisition of the satellite images (section 3.1), 2) data preprocessing (section 3.2), and 3) NDVI analysis (section 3.3).

3.1. Acquisition of the satellite images

The satellite images from the collection Level-2A of the European Space Agency Sentinel-2 mission (`https://sentinel.esa.int`) were used this study. This data product offers multiband atmospherically-corrected surface reflectance images covering the visible and infrared spectrum at 10-m resolution. The subweekly revisit time of the satellite usually provides a sufficiently dense cloud-free image time series to monitor the seasonal change in mountain pastures.

All available images of the study region were acquired for the time span of 2016-2023 to analyze the seasonal growth over eight years. We used the download routine of the open-source platform EOdal [41]. EOdal retrieves the images by querying the Microsoft Planetary Computer Data Catalog (`https://planetarycomputer.microsoft.com/catalog`) with the protocol STAC (`https://stacspec.org`). For the big amount of images and the large area covered (1115 km^2), the EOdal code was adapted to run iteratively making separate queries to the data catalog and to download the images in data chunks stored locally. This also allows distributing the download process and pausing/resuming in case of server errors. In addition, preliminary data-treatment operations were applied in this phase. See the complete downloading workflow in appendix Appendix A.

3.2. Data Preprocessing

In order to extract the growth pattern of the pasture habitats from the NDVI time series, the acquired images were preprocessed with a novel workflow to obtain a database for pixel analysis. In the database, every pixel is associated to different attributes, including its NDVI value, habitat, spatial coordinates, shadow label, elevation, aspect, and time stamp. See appendix Appendix B for more information.

3.3. Annual growth curve analysis

The annual growth curves of the habitats were extracted for all available years (2016-2023) and plotted. To better isolate the growth pattern from disturbances and scatter related to the complex topography, only pixels facing southward (aspect angle between 90 and 270 degrees) and outside the mountain shadow (shadow label = 0) were considered. The growth curves were then generated for different classes of altitude to study the dependency of growth on the elevation change.

For every annual set of NDVI values (example in Figure 2), a growth curve representing the central tendency was derived from the daily medians and a variability envelope was computed from the daily 0.25 and 0.75 quantiles. This excluded outlier pixel data, common in satellite images. The curve values were interpolated at every Day of The Year (DOY) using the piecewise interpolation Pchip [42] (`https://docs.scipy.org/doc/scipy/reference/generated/scipy.interpolate.pchip_interpolate.html`). This technique was chosen for its stability since it preserves a smooth interpolation, but also local monotonicity among data points.

From the obtained growth curves, the following statistical indicators were computed to describe the growth season. The Start Of Greening (SOG) was defined empirically as the DOY when the median growth curve goes above the prescribed threshold of 0.05 for more than 5 days, marking a stable transition to positive the positive NDVI range, corresponding to growing vegetation. Similarly, the End Of Season (EOS) occurs when the curve goes below the same threshold for five days. The Area Under the Curve, commonly used in NDVI analysis [e.g. 34, 43, 44, 45] and considered as a proxy for the cumulative pattern of growth in grassland, was computed first for the first portion of the growth season (AUC1). This is delimited by the SOG and the mid-season, defined as the 1-st of August, generally half-away from the reach of the curve plateau to the start of the senescence (declining of the curve). The same indicator was computed for the second half of season (AUC2), from mid-season until the EOS, and for the whole season (AUC), from the SOG

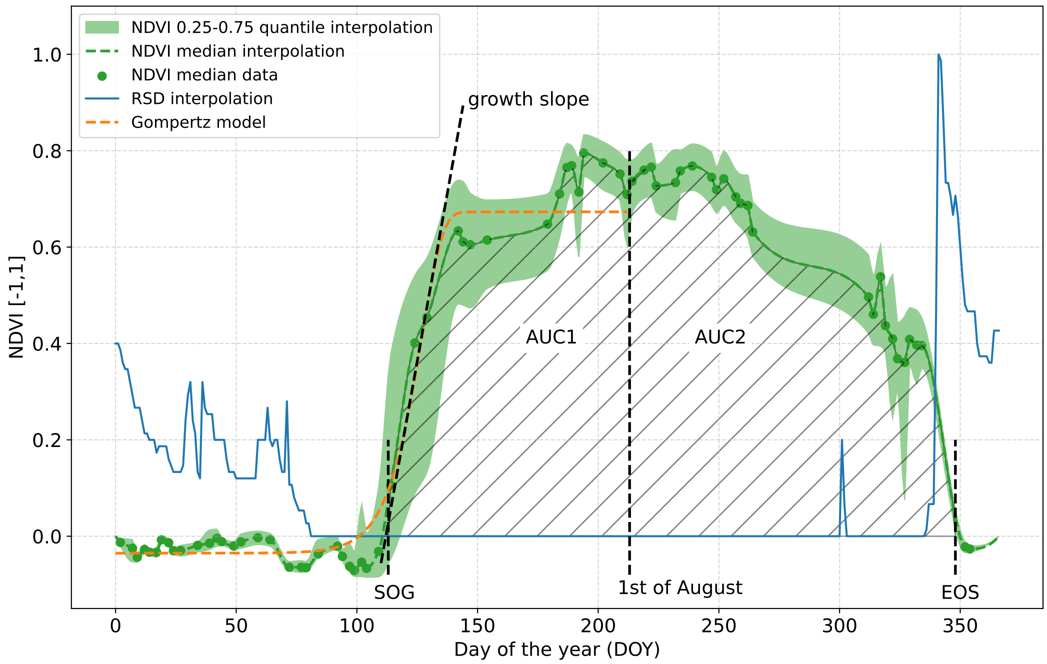

Figure 2: Sketch of the annual curve obtained from a selected sample of NDVI data, as a function of the day of the year (DOY), with the following statistical indicators: elements in black are the derived curve indicators, namely: the Start Of Greening (SOG) and End Of Season (EOS) days, the growth slope derived from the fitted Gompertz model (orange line), the Areas Under the Curve for the first (AUC1) and second (AUC2) halves of season. The blue line indicates the relative snow depth (RSD).

to the EOS. AUC1 and AUC2 are computed for the 0.25 and 0.75 quantile curves as well.

In addition, the initial slope of the growth curve was modeled using the Gompertz function similarly to [46]. This sigmoidal type of curve (orange line in Figure 2), suitable to represent growth processes, was formulated here with the following equation:

$$y = a \exp\{-\exp[c(x-b)]\} + d \tag{1}$$

with y being the fitted NDVI value, x the DOY, a the curve amplitude parameter, b the x coordinate of the sigmoid flex point, c the growth slope factor, and d the y coordinate of the maximum growth plateau. The function was fitted with a least-square method on the Pchip interpolation of the data, since it preserves a more stable fitting in case of scarce NDVI data in the year. The following parameter boundaries were imposed to preserve a realistic shape of the NDVI growing curve: $[0, 2]$ for a, with 0 for zero curve amplitude (no growth) and 2 for the maximum NDVI theoretical amplitude from -1 to 1, $[50, 200]$ for b, limiting the center of the growing slope between DOY 50 and 200, $[0, 1]$ for c, with 0 for horizontal slope and 1 for vertical slope, and $[0, 1]$ for d, with 0 for the curve maximum equal to zero (no growth) and 1 for the maximum equal to 1 (NDVI theoretical maximum).

3.4. Comparison of seasonal indicators

The seasonal indicators derived from the growth curves were then compared among different units and classes of elevation and their reciprocal correlation is investigated. The AUC versus elevation correlation could be computed on the single parcels, leading to large ensembles of point sets. Conversely, the descriptors based on the Gompertz function (growth slope and growth maximum), being the function fitting sensible to the data amount used, are computed from the entire pixel ensembles per habitat and year, leading to more stable curve shapes. On the other hand, this lead to only eight data points (one per year), more prone to non significant correlation values. For this reason, the Student test p-value for the null hypothesis of non-correlation [47] was computed to check the significance of the estimated correlation coefficients. Following the common practice for this test, correlation coefficients with p-values lower than 0.05 were considered significant.

4. Results

4.1. Annual growth curves

Examples of annual growth curves extracted for every habitat for 2019 and 2020 are shown in Figure 3. The two years demonstrate clear differences representative of the variations which can be similarly found among other years (supplemental material 1). For both 2019 and 2020, the majority of the habitats present annual curves with a relatively low NDVI variability (about $\pm$ 0.05) around the median (dashed line), as indicated by the 0.25-0.75 quantile envelope. Conversely, resting areas and tall shrubs (Figure 3 c and i) show a larger NDVI variability around $\pm$ 0.1. Mesic, wet pastures, and wetlands (Figure 3 a, b, f, and g) reach NDVI 0.8 in full season, while dry pastures (d), acidic ones (e), and resting areas (d) present a lower NDVI plateau. The growth curves of dwarf and tall shrubs (Figure 3 h and i) present a larger plateau with values mainly between 0.6 and 0.8, and a sharper end of season instead of a gradual senescence.

Interannual variations in the habitat growth are well represented by the differences between 2019 (Figure 3 blue) and 2020 (orange) curves. Those primarily regard the season length delimited by the SOG and the EOS (Figure 2). In particular, the SOG occurs when winter snow disappears, as shown by the RSD time series (Figure 3 continuous lines). Similarly the EOS occurs

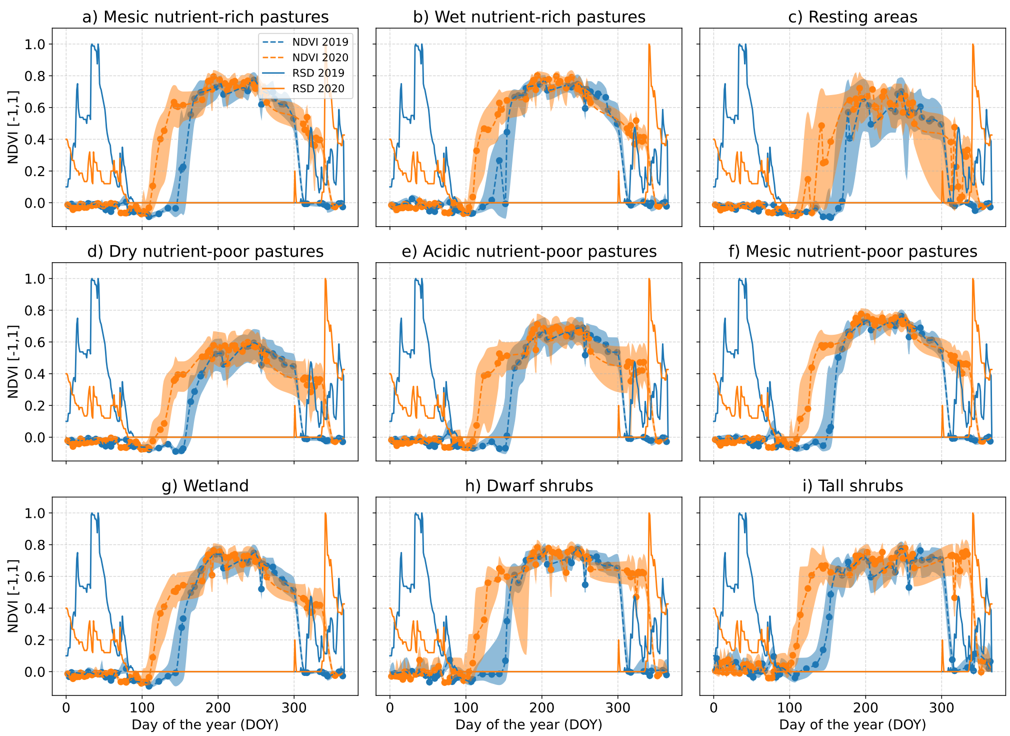

Figure 3: Example of NDVI (dashed lines and envelopes) and RSD (continuous lines) annual curves in two compared years: 2019 (blue) and 2020 (orange). For NDVI, the variability envelope is delimited by the the 0.25 and 0.75 quantiles of the daily pixel-value distribution, while the dashed line represents the median.

with the beginning snowfall towards the end of the year. For all habitats, the 2019 growth season is shorter since delimited by a more persistent snow in spring (late SOG) and earlier snow arrival in fall (early EOS). This variation does not visibly affect the maximum growth, but rather the area under the curve (AUC), whose variations are analysed in the following section.

4.2. Seasonal growth and elevation

The seasonal growth is analysed by means of the NDVI AUC (see section 3.3) for the first (AUC1) and second (AUC2) halves of the season. These are computed (Figures 4 and 5 panels a) for every unit (colors), four classes of elevation (separated by vertical grid lines), and the eight available years (2016-2023, adjacent bars of the same color) from the median (dots) and 0.25-0.75 quantile (error bars) annual curves. A descending trend in the AUC1 (Figure 4 a) is observed when elevation increases, dropping from the 20-60 range at 2000-2200 m a.s.l., to 0-40 at 2600-2800 m. A similar trend is observed for AUC2 (Figure 5 a). In both season halves and for lower altitudes (2000-2200 m), mesic and wet habitats (green shades, orange, red, and blue colors) present the largest AUC among pastures, mainly in the range 40-80. Conversely, lower AUC values mainly in between 20 and 50 belong to dry pastures (yellow), resting areas (purple), and tall shrubs (brown) present the lowest values. These differences even out along the elevation profile, until above 2600 m where all units AUC1 mainly vary in 0-40 for the first part of the season and in 30-60 for AUC2.

Tall shrubs (Figure 4 and 5 brown color) keep distinctly higher and variable AUC values with elevation, mainly between 50 and 100, and disappear above 2400 m a.s.l., above the treeline. Conversely, dwarf shrubs (beige color) present AUC values comparable to wet pastures and persist up to 2600 m of elevation.

The vertical error bars in the panels a) of Figures 4 and 5, defined by the AUC of the 0.25-0.75 curves, are based on the variability in daily pixel ensembles. The length of these bars (interquartile range) is therefore related

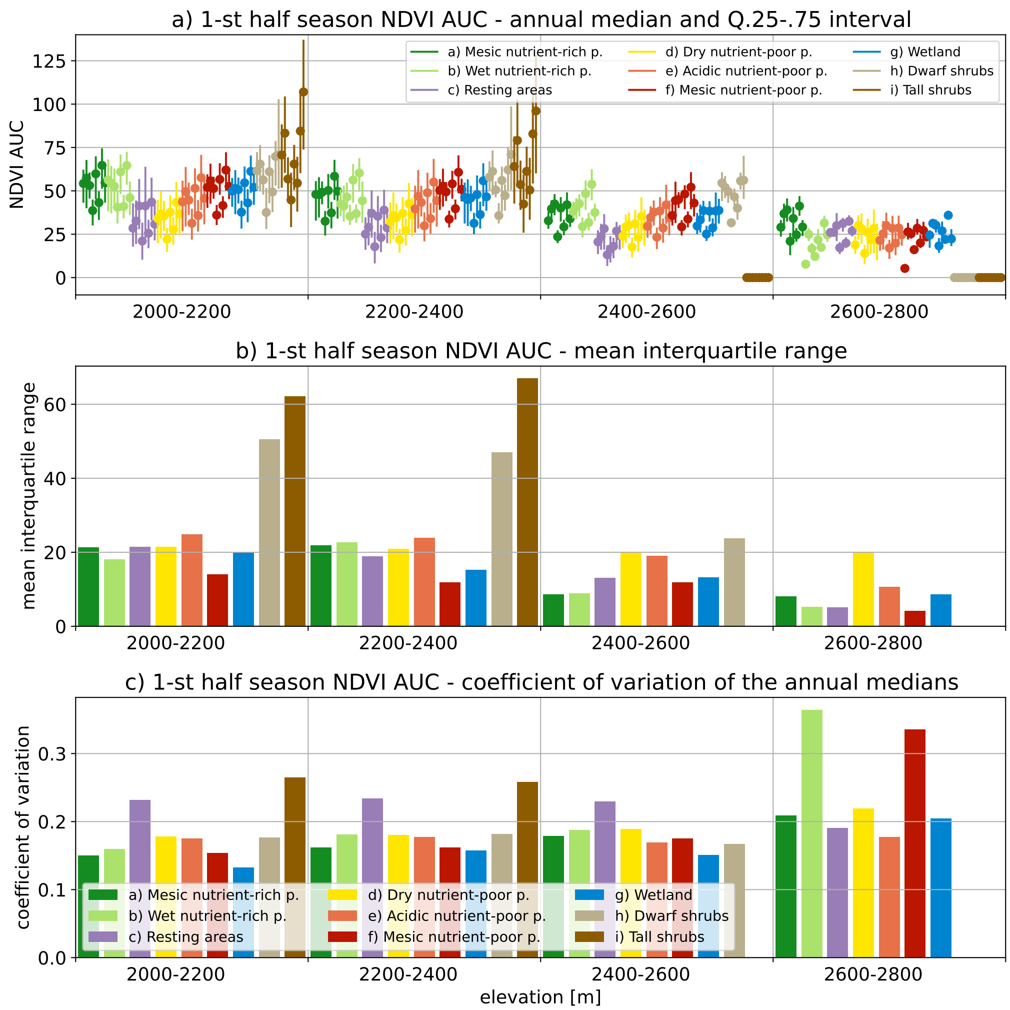

Figure 4: Plot of the NDVI AUC for the first half of the growth season (see section 3.3) for different habitat units (different colors), years (same color bars), and elevation classes (separated by vertical grid lines): a) annual median (dots) and .25-.75 quantile envelope (error bar) for different years (2016-2023), b) mean interquartile range (equivalent to the mean error bar length in a), and c) coefficient of variation of the annual medians (dots in a) for every unit.

to the spatial variability of the unit growth during the year. The means of this quantity (among different years) are displayed again as bars in Figures 4 and 5 panels b). For the first season half, tall and dwarf shrubs present a sensibly large spatial variability in the growth, with a mean interquartile above 60 and 40 respectively. Conversely, the other habitats vary mainly between 20 and 30. These values tend to diminish sensibly with elevation above 2400 m, partly due to the decrease of available pixels in high elevation. For the second half of the season (Figure 4 b), resting areas (purple color) stand out with a mean interquartile range around 25 while the other habitats range between 10 and 17. Similarly to the first season half, these differences reduce above 2400 m of elevation.

The panels c of Figures 4 and 5 display the coefficient of variation among the AUC median curves of the different years considered (dots in panels a of the same figures). This indicator represents the relative interannual variation of the AUC for the different units and elevation classes. For the first half season (Figure 4 c) and up to 2600 m, resting areas and tall shrubs present a coefficient of variation higher than 0.2 while all other units mainly lie between 0.1 and 0.2. This pattern changes above 2600 m, where wet nutrient-rich pastures (light green) and mesic nutrient-poor ones (red) present a sensibly higher coefficient of variation above 0.3, while all other units range around 0.2. In the second half of the season (Figure 4 c), the interannual coefficient of variation mainly varies between 0.1 and 0.15 for all units with no clear pattern in function of altitude.

The dependency of the habitat growth upon elevation changes is investigated further by computing the Pearson correlation coefficient r between the

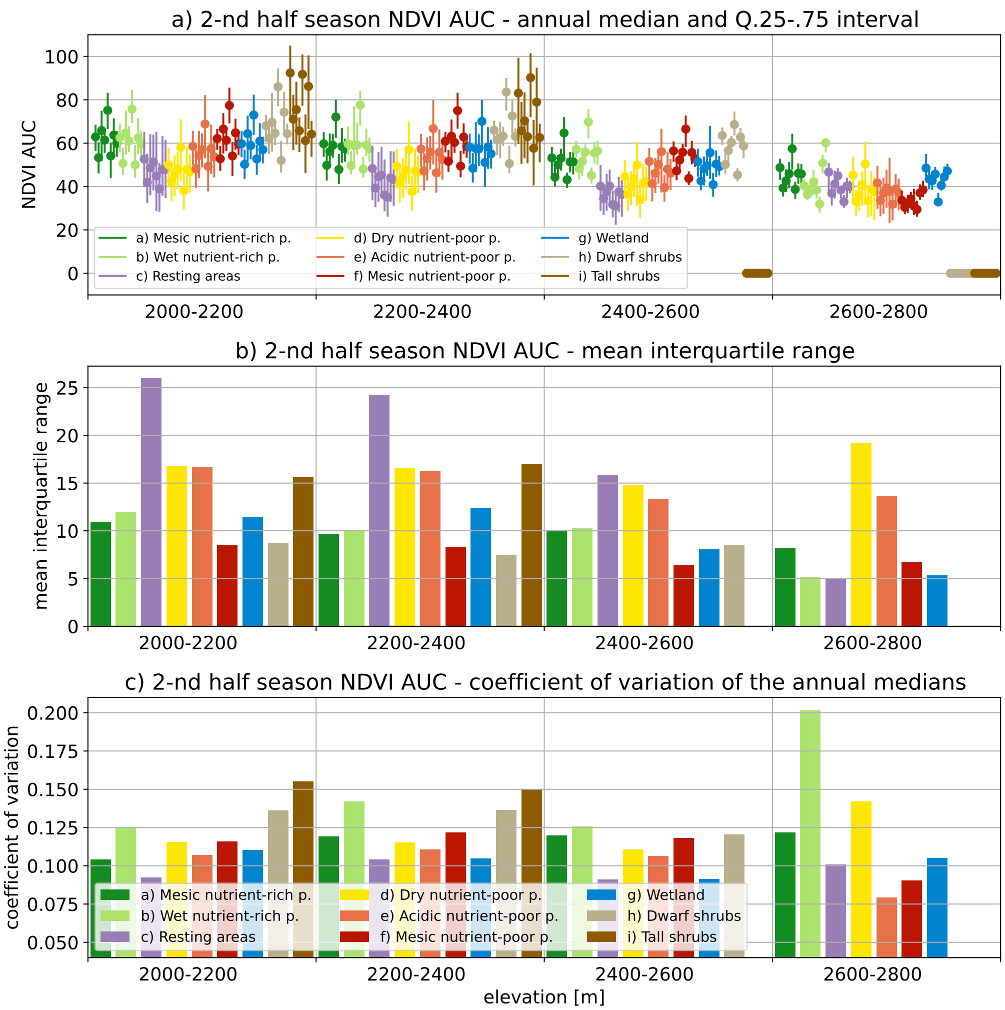

Figure 5: Plot of the NDVI AUC for the second half of the growth season (see section 3.3) for different habitat units (different colors), years (same color bars), and elevation classes (separated by vertical grid lines): a) annual median (dots) and .25-.75 quantile envelope (error bar) for different years (2016-2023), b) mean interquartile range (equivalent to the mean error bar length in a), and c) coefficient of variation of the annual medians (dots in a) for every unit.

AUC for all parcels and their median elevation (Table 2) in both the first and second season halves. Parcels presenting less than five points in the annual AUC curve were discarded to minimize biased AUC values. In general, negative correlation is found, meaning that all habitats grow less with elevation. Moreover, dry and acidic nutrient-poor pastures present significantly high correlation values for almost all years, on average higher than 0.8 in the first half of the season and higher than 0.7 in the second half, and with a low standard deviation among the years (Table 2 mean and std columns). Resting areas and dwarf shrubs growth present a weak (0.5 - 0.65) correlation. This suggests that the growth of these units is dependent on elevation changes.

4.3. Growth dynamics

The statistical descriptors of the growth curves, described in section 3.3, are put in relation by computing the Pearson correlation coefficient (Table 3). Among the tested combinations of descriptors, $r_{g,s}$ (SOG vs growth slope) is significantly high and positive for all pasture units and resting areas, meaning that a later SOG (higher value) is associated to a higher growth slope. Both quantities are anticorrelated to the first season half AUC, decreasing when the SOG and slope increase, as shown by the negative coefficients $r_{g,a1}$ and $r_{s,a1}$. Moreover, all pasture habitats show a significant positive correlation between the AUC2 and the EOS ($r_{a2,e}$).

The growth curves of the wetland habitat present a weaker but similar correlation pattern as the other pastures. Conversely, dwarf and tall shrubs only show the AUC2 correlated to the EOS ($r_{a2,e}$), with a stronger value of 0.9 for dwarf shrubs and a weaker one of 0.73 for tall shrubs.

Table 2: Pearson correlation coefficient (r) of the median NDVI AUC versus median elevation for different habitat units, computed from every parcel and both the first and second halves of season. The mean (mean) and standard deviation (std) columns refer to the annual correlation values on the left. Values higher/lower than ±0.6 are marked in bold.

Unit	2016	2017	2018	2019	2020	2021	2022	2023	mean	std
First Season half										
Mesic nutrient-rich pastures	-0.53	-0.51	-0.48	-0.50	-0.55	-0.55	-0.45	-0.53	-0.51	0.033
Wet nutrient-rich pastures	-0.47	-0.38	-0.43	-0.42	-0.51	-0.44	-0.29	-0.37	-0.41	0.063
Resting areas	**-0.74**	**-0.61**	-0.59	-0.58	**-0.66**	**-0.65**	-0.48	**-0.60**	-0.61	0.070
Dry nutrient-poor pastures	**-0.82**	**-0.80**	**-0.79**	**-0.87**	**-0.83**	**-0.81**	**-0.77**	**-0.82**	-0.81	0.027
Acidic nutrient-poor pastures	**-0.80**	**-0.78**	**-0.80**	**-0.83**	**-0.81**	**-0.83**	**-0.76**	**-0.80**	-0.80	0.022
Mesic nutrient-poor pastures	-0.54	-0.41	-0.48	-0.42	-0.52	-0.51	-0.38	-0.46	-0.46	0.052
Wetland	-0.56	-0.42	-0.40	-0.49	-0.45	-0.49	-0.34	-0.45	-0.45	0.062
Dwarf shrubs	-0.27	**-0.66**	**-0.67**	**-0.70**	**-0.73**	**-0.66**	**-0.68**	**-0.63**	-0.62	0.136
Tall shrubs	-0.26	-0.02	-0.17	-0.14	-0.19	-0.30	0.02	0.12	-0.11	0.135
Second season half										
Mesic nutrient-rich pastures	-0.36	-0.57	-0.20	-0.39	-0.28	-0.38	-0.38	-0.53	-0.38	0.113
Wet nutrient-rich pastures	-0.30	-0.48	0.04	-0.32	-0.18	-0.26	-0.10	-0.36	-0.24	0.153
Resting areas	-0.47	**-0.67**	-0.34	-0.52	-0.47	-0.47	-0.36	**-0.67**	-0.49	0.115
Dry nutrient-poor pastures	-0.57	**-0.75**	**-0.64**	-0.56	**-0.73**	-0.57	**-0.71**	-0.58	-0.63	0.073
Acidic nutrient-poor pastures	**-0.69**	**-0.75**	**-0.70**	**-0.70**	**-0.75**	**-0.76**	**-0.74**	**-0.76**	-0.73	0.028
Mesic nutrient-poor pastures	-0.33	-0.55	-0.15	-0.57	-0.16	-0.35	-0.26	**-0.64**	-0.37	0.177
Wetland	-0.34	-0.36	-0.12	-0.31	-0.15	-0.35	-0.29	-0.40	-0.29	0.093
Dwarf shrubs	-0.44	-0.39	-0.07	-0.20	-0.44	-0.27	-0.54	-0.37	-0.33	0.141
Tall shrubs	0.03	-0.33	-0.13	-0.10	0.07	0.05	-0.02	-0.44	-0.10	0.173

5. Discussion

5.1. Methodological considerations

In the present paper, a satellite-based time series analysis on mountain grassland ecosystem was developed to investigate the variability of different pasture and shrub habitats across different years and altitudes. The inves-

Table 3: Correlation coefficients r_{xy}, where x and y are growth curve descriptors (section 3.3), namely: SOG (g), growth slope (s), AUC1 ($a1$), AUC2 ($a2$), EOS (e), curve maximum (m). Bold values indicate significant correlation coefficients (p-value < 0.05).

Unit	$r_{g,s}$	$r_{g,a1}$	$r_{g,m}$	$r_{g,a2}$	$r_{g,e}$	$r_{s,a1}$	$r_{s,m}$	$r_{s,a2}$
Mesic nutrient-rich p.	**0.85**	**-0.93**	0.09	-0.14	-0.22	-0.71	-0.16	0.29
Wet nutrient-rich p.	**0.93**	**-0.82**	-0.01	-0.33	-0.40	**-0.76**	-0.07	-0.18
Resting areas	**0.82**	**-0.92**	-0.31	-0.50	-0.61	-0.69	-0.39	-0.17
Dry nutrient-poor p.	**0.90**	**-0.89**	-0.29	-0.20	-0.40	**-0.75**	-0.49	-0.02
Acidic nutrient-poor p.	**0.83**	**-0.92**	0.07	-0.16	-0.41	**-0.75**	-0.33	0.15
Mesic nutrient-poor p.	**0.85**	**-0.93**	0.20	-0.23	-0.33	**-0.79**	-0.13	0.21
Wetland	**0.74**	**-0.85**	0.19	0.03	-0.13	-0.41	-0.18	0.61
Dwarf shrubs	0.10	-0.16	-0.37	0.28	0.51	-0.70	-0.48	-0.03
Tall shrubs	-0.02	-0.24	-0.30	0.41	0.06	0.07	-0.65	0.06

Unit	$r_{s,e}$	$r_{a1,m}$	$r_{a1,a2}$	$r_{a1,e}$	$r_{m,a2}$	$r_{m,e}$	$r_{a2,e}$
Mesic nutrient-rich p.	0.24	0.08	0.34	0.40	-0.10	-0.30	**0.92**
Wet nutrient-rich p.	-0.24	0.09	0.57	0.69	0.14	-0.20	**0.90**
Resting areas	-0.27	0.46	0.35	0.50	0.23	0.17	**0.87**
Dry nutrient-poor p.	-0.08	0.52	0.30	0.49	-0.04	-0.18	**0.90**
Acidic nutrient-poor p.	-0.05	0.07	0.30	0.54	-0.20	-0.43	**0.87**
Mesic nutrient-poor p.	0.14	0.02	0.37	0.45	-0.02	-0.24	**0.93**
Wetland	0.51	-0.07	0.32	0.45	-0.31	-0.54	**0.91**
Dwarf shrubs	-0.01	0.09	0.33	0.32	-0.06	-0.09	**0.90**
Tall shrubs	0.53	0.23	0.07	0.11	-0.26	-0.54	**0.73**

tigation was based on the high-resolution satellite Sentinel-2 images which constitute the current freely available state-of-the-art product with an optimal balance among spatial resolution, sensor quality, temporal coverage, and revisit time. Data acquisition based on EOdal allowed systematic access to the entire image time-series for a large ROI. The use of a data dictionary for the NDVI pixel analysis allowed dealing with the complex influencing factors linked to topography in a much more agile way than considering whole image cubes.

For the considered region, Sentinel-2 only delivers complete annual time series since 2016. Still, that allowed to investigate eight years of data with their corresponding weather variations. This time span offers a rather variable snow persistence for the study region, depending on winter precipitation and temperatures. The snowpack melt date, measured at the Scuol station (see section 2.1), varies between the beginning of April (2017) and the end of May (2021). Nevertheless, in order to investigate long term trends, some decades of images would be needed to be reliable and representative. In addition, periodical updates of the habitat survey map would be necessary to inform about changes in the vegetation spatial distribution. Finally, remote sensing data are always a proxy information for physiological processes, with the advantage to cover wide areas but the need of experimental confirmation from in situ data. In particular, NDVI should be only considered informative of the growth pattern and not to make estimations or comparison in terms of absolute growth values, which are linked to different physiological traits of species [48].

5.2. Two types of pasture growth dynamics

With the present NDVI analysis, we identified two main types of growth patterns, belonging to dry and wet pastures respectively. This difference, as explained in the following, is linked to the vegetation response to weather and elevation changes.

As suggested by the AUC statistics (Figures 4 and 5), mesic and wet pasture habitats present a larger cumulative growth and less variable in space compared to dry pastures and resting areas during the whole growth season at altitudes from 2000 to 2400 m a.s.l. At higher elevation, we observed a generalized reduction of these differences. This homogenization of pasture growth among years and vegetation types can be explained by water scarcity and lower temperature conditions usually found at mountain tops.

5.3. Dependence of growth on elevation

The parcel-wise analysis of the AUC in relation to elevation (Table 2) reveals a significant correlation between growth and elevation in dry and less productive pasture habitats. These habitats are probably more dependent on hydroclimatic variations (thermal lapse and soil humidity rates) along the elevation profile. Growth in the first half of the season appears to be consistently more dependent on elevation with respect to growth in the second half. Conversely, wetter habitats, more frequently present along valley axes, may be affected more strongly by hydroclimatic and geomorphological conditions. It is the case for orographic precipitation regimes and wind exposure controlled by the valley orientation and morphology, or soil type and thickness [49].

5.4. Impact of annual weather variability on growth

Interannual weather variations turn out to be important for growth in pasture habitats, with growth curve AUC variations of 15-20 %, more pronounced in the first part of the season (Figures 4 and 5 panels c). There is no strong difference of this variation depending on the vegetation type, with only resting areas tending to be moderately more vulnerable than the other habitats.

The statistical descriptors of the growth curves (Table 3) allow analysing the growth dynamics of the vegetation in the mountain rangeland ecosystem. Pastures units with delayed start of the growth season, controlled by snow persistence, show an increase of the growth slope ($r_{g,s}$). This suggests a compensation in the growth process by increased growth speed after late snow melt. These dynamics may be explained by mechanisms of damping snow persistence variations, observed in plot-scale studies in alpine meadow and tundra ecosystems, for example benefiting of a high temperature after late snow melt [50], or belowground processes and undersnow growth [51, 52, 53, 54].

Nevertheless, both the EOS and the growth slope are negatively correlated with the AUC in the first part of the season ($r_{g,a1}$ and $r_{s,a1}$), suggesting that the mentioned compensation mechanism, faster growth after late-melting snow, does not fully recover the lack of assimilation due to a shorter season. Therefore, in agreement to previous investigations [55, 56], snow persistence still appear as one main controlling factor on the first half of the growth season amplitude and productivity. Similarly, autumn snow occurrence ends the season and limits growth in pastures, as suggested by the correlation between the AUC2 and EOS $r_{a2,e}$, with the EOS being linked to the first snow occurrence (see Figure 2). Also, growth in the second season half appears to be rather independent from the first half (low $r_{a1,a2}$).

5.5. Shrub habitats: a matter of tallness

The two analyzed shrub habitats show different AUC statistics (Figures 4 and 5 beige and brown colors). Although being present in our ROI only up to 2400m, tall shrubs present the highest growth curve values among all habitats with no big variations in the AUC in function of elevation. Since tall vegetation does not cope well with low air temperature and wind-driven heat loss [57], thermal excursion may be the main limiting factor for their growth at high elevation. Conversely, dwarf shrubs present lower growth values comparable to pasture habitats and moderately correlated with elevation changes (Table 2).

Both shrub types vary twice more their growth in space than pastures in the first half of the season (Figures 4 panel b) and tall ones show substantial interannual variations of the seasonal biomass production (15 and 25 % among 2016-2023 AUC1 and ACU2 medians) in response to annual weather fluctuations (Figures 4 and 5 panels c).

While, with both shrub types, there isn't a significant correlation between cumulative growth and the variation of the SOG, the arrival of snow in autumn (EOS) seems to limit more importantly their growth ($r_{a2,e}$ in Table 3).

6. Conclusions

In this paper, we presented a high-resolution satellite image analysis focused on the characterization of nine habitats in mountain rangelands. The study is based on the satellite product Sentinel-2 and the habitat map of the mountain pastures surrounding the Swiss National Park (Grisons canton, Switzerland).

A pixel analysis method was developed to derive the growth pattern of the small-scale habitat in a complex topographic setting. Based on the spectral index NDVI, the workflow allowed analysing the growth season habitats in relation with elevation and snow persistence.

The main findings of this study are that wet and dry pastures exhibit two main different growth patterns: the former more productive at mid elevation, the latter growing more variably in space and more sensitive to elevation. Also, snow melt, controlling the beginning of the growing season, is the main limiting factor for the cumulative growth of all pasture habitats. This delay is partially compensated by a quicker growth in late-snow-melting years. Similarly, the arrival of snow in autumn limits the accumulation of biomass in the second part of the season. These dynamics at the end of the season also affects dwarf shrubs, while tall ones green variably in space and independently from elevation until the treeline. For all habitats, interannual weather fluctuations impact growth importantly, with 15-20 % of AUC variation.

These findings, in agreement with previous ground-truthing studies, expand the knowledge of habitat seasonality and their response to change in hydro-climate factors, in particular snow persistence.

Possible improvements and applications of this study include the comparison of the findings from on-site plot analysis and growth models, and the extension to other alpine areas. The growth curve descriptors can be to spatialized to compile thematic maps of SOG, EOS, and productivity indicators. This cartographic product is a useful tool to plan rangeland management, together with an in-depth analysis of climate factors to predict seasonal productivity.

Code availability

Scripts to acquire, preprocess, and analyze the satellite images: `https://github.com/EOA-team/Satellite_monitoring_of_mountain_pastures` Python-dem-shadow package with usage example: `https://github.com/EOA-team/python-dem-shadows`

Appendix A. Downloading workflow for Sentinel-2 images

The workflow developed for the programmatic retrieval of the Sentinel-2 images consists in the following steps:

1. According to the parameters set for the EOdal mapper, the Sentinel-2 data catalog is queried for a given time span and ROI with the STAC protocol `https://stacspec.org`. A series of sub-queries to divide the image time series in data chunks.
2. For every data chunk, the sub-query is sent to the server and the images are downloaded.

3. Within the EOdal preprocessing module, all image pixels classified as any cloud type or non-vegetation cover are masked. this is done according to the Sentinel-2 Scene Classification Layer (SCL), available as raster band for every image. In this case, snow pixels were not masked since they include mixed-spectrum values allowing to better observe the early growth of the vegetation units.
4. All bands in every image is projected on a defined target grid of 10 m resolution (in line with Sentinel-2 resolution) covering the ROI in the Swiss local CRS CH1902/LV95 (EPGS:2056). This leads to a 4D data cube for every data chunk, whose dimensions consists in xy image coordinates, number of bands, and different temporal frames.
5. For every data cube, the NDVI images are computed using Sentinel-2 red (B04) and near-infrared (B08) bands with the standard formula NDVI = (B08-B04)/(B08+B04). This leads to a 3D NDVI cube consisting in xy image coordinates and temporal frame.
6. Every data cube is stored locally.

Appendix B. Preprocessing workflow for the NDVI images

The obtained NDVI images are preprocessed as follows. First, the pasture classification map (section 2) of the ROI is projected on the same xy grid of the NDVI cube. The same is done for the DEM and the aspect is derived from it using the richdem python package (`https://richdem.com/`). These two raster variables are then used in the following steps, run iteratively on every NDVI data cube (section 3.1):

1. The NDVI cube is loaded in python.

2. Using the rasterized habitat map, images are discarded if they contain less than 10% pixels informed among the ones mapped as habitat units. This allows avoiding too biased point values in the extracted annual growth curves.
3. For every accepted image, the shadow cast by mountains is computed using the package python-dem-shadow (adapted script in the Code Availability section). This way, every pixel is labeled as covered by shadow or not.
4. From the DEM, the aspect of every pixel was derived using the python package richdem (`https://pypi.org/project/richdem/`).
5. Pixels mapped as habitat units are extracted from every image and stored in a python dictionary, where every item represents an attribute linked to pixels and contains a vector of values, one for each pixel.

More information on the dataset structure is available in the documentation of the attached code (section 6).

References

[1] B. Hoersch, G. Braun, U. Schmidt, Relation between landform and vegetation in alpine regions of Wallis, Switzerland. A multiscale remote sensing and GIS approach, Computers, Environment and Urban Systems 26 (2-3) (2002) 113–139. doi:10.1016/S0198-9715(01)00039-4. URL https://linkinghub.elsevier.com/retrieve/pii/S0198971501000394

[2] A. Becker, C. Körner, J.-J. Brun, A. Guisan, U. Tappeiner, Ecological and land use studies along elevational gradients, Mountain Research and

Development 27 (1) (2007) 58–65. doi:10.1659/0276-4741(2007)27[58:EALUSA]2.0.CO;2.
URL http://www.bioone.org/doi/abs/10.1659/0276-4741%282007%2927%5B58%3AEALUSA%5D2.0.CO%3B2

[3] C. Schwörer, D. Colombaroli, P. Kaltenrieder, F. Rey, W. Tinner, Early human impact (5000–3000 BC) affects mountain forest dynamics in the A lps, Journal of Ecology 103 (2) (2015) 281–295. doi:10.1111/1365-2745.12354.
URL https://besjournals.onlinelibrary.wiley.com/doi/10.1111/1365-2745.12354

[4] D. MacDonald, J. Crabtree, G. Wiesinger, T. Dax, N. Stamou, P. Fleury, J. Gutierrez Lazpita, A. Gibon, Agricultural abandonment in mountain areas of Europe: Environmental consequences and policy response, Journal of Environmental Management 59 (1) (2000) 47–69. doi:10.1006/jema.1999.0335.
URL https://linkinghub.elsevier.com/retrieve/pii/S0301479799903353

[5] T. Dirnböck, S. Dullinger, G. Grabherr, A regional impact assessment of climate and land-use change on alpine vegetation, Journal of Biogeography 30 (3) (2003) 401–417. doi:10.1046/j.1365-2699.2003.00839.x.
URL https://onlinelibrary.wiley.com/doi/10.1046/j.1365-2699.2003.00839.x

[6] G. Cocca, E. Sturaro, L. Gallo, M. Ramanzin, Is the abandonment of traditional livestock farming systems the main driver of mountain land-

scape change in alpine areas?, Land Use Policy 29 (4) (2012) 878–886. doi:10.1016/j.landusepol.2012.01.005.
URL https://linkinghub.elsevier.com/retrieve/pii/S0264837712000075

[7] R. Engler, C. F. Randin, W. Thuiller, S. Dullinger, N. E. Zimmermann, M. B. Araújo, P. B. Pearman, G. Le Lay, C. Piedallu, C. H. Albert, P. Choler, G. Coldea, X. De Lamo, T. Dirnböck, J.-C. Gégout, D. Gómez-García, J.-A. Grytnes, E. Heegaard, F. Høistad, D. Nogués-Bravo, S. Normand, M. Puşcaş, M.-T. Sebastià, A. Stanisci, J.-P. Theurillat, M. R. Trivedi, P. Vittoz, A. Guisan, 21st century climate change threatens mountain flora unequally across europe: Climate change impacts on mountain florae, Global Change Biology 17 (7) (2011) 2330–2341. doi:10.1111/j.1365-2486.2010.02393.x.
URL https://onlinelibrary.wiley.com/doi/10.1111/j.1365-2486.2010.02393.x

[8] Q. Du, Y. Sun, Q. Guan, N. Pan, Q. Wang, Y. Ma, H. Li, L. Liang, Vulnerability of grassland ecosystems to climate change in the Qilian mountains, Northwest China, Journal of Hydrology 612 (2022) 128305. doi:10.1016/j.jhydrol.2022.128305.
URL https://linkinghub.elsevier.com/retrieve/pii/S0022169422008770

[9] G. Grabherr, M. Gottfried, H. Pauli, Climate change impacts in alpine environments, Geography Compass 4 (8) (2010) 1133–1153. doi:10.1111/j.1749-8198.2010.00356.x.

URL https://compass.onlinelibrary.wiley.com/doi/10.1111/j.1749-8198.2010.00356.x

[10] J. G. Ernakovich, K. A. Hopping, A. B. Berdanier, R. T. Simpson, E. J. Kachergis, H. Steltzer, M. D. Wallenstein, Predicted responses of arctic and alpine ecosystems to altered seasonality under climate change, Global Change Biology 20 (10) (2014) 3256–3269. doi:10.1111/gcb.12568.
URL https://onlinelibrary.wiley.com/doi/10.1111/gcb.12568

[11] B. Deroche, P. Pradel, R. Baumont, Long-term evolution and prediction of feed value for permanent mountain grassland hay: Analysis of a 32-year data set in relation to climate change, Grass and Forage Science 75 (1) (2020) 18–27. doi:10.1111/gfs.12465.
URL https://onlinelibrary.wiley.com/doi/10.1111/gfs.12465

[12] E. R. Frei, J. Ghazoul, P. Matter, M. Heggli, A. R. Pluess, Plant population differentiation and climate change: Responses of grassland species along an elevational gradient, Global Change Biology 20 (2) (2014) 441–455. doi:10.1111/gcb.12403.
URL https://onlinelibrary.wiley.com/doi/10.1111/gcb.12403

[13] D. W. Inouye, Effects of climate change on alpine plants and their pollinators, Annals of the New York Academy of Sciences 1469 (1) (2020) 26–37. doi:10.1111/nyas.14104.
URL https://nyaspubs.onlinelibrary.wiley.com/doi/10.1111/nyas.14104

[14] M. Wachendorf, T. Fricke, T. Möckel, Remote sensing as a tool to assess botanical composition, structure, quantity and quality of temperate grasslands, Grass and Forage Science 73 (1) (2018) 1–14. doi:10.1111/gfs.12312.
URL https://onlinelibrary.wiley.com/doi/10.1111/gfs.12312

[15] B. Taylor, P. Dini, J. Kidson, Determination of seasonal and interannual variation in New Zealand pasture growth from NOAA-7 data, Remote Sensing of Environment 18 (2) (1985) 177–192. doi:10.1016/0034-4257(85)90047-1.
URL https://linkinghub.elsevier.com/retrieve/pii/0034425785900471

[16] C. Raab, F. Riesch, B. Tonn, B. Barrett, M. Meißner, N. Balkenhol, J. Isselstein, Target-oriented habitat and wildlife management: Estimating forage quantity and quality of semi-natural grasslands with Sentinel-1 and Sentinel-2 data, Remote Sensing in Ecology and Conservation 6 (3) (2020) 381–398. doi:10.1002/rse2.149.
URL https://zslpublications.onlinelibrary.wiley.com/doi/10.1002/rse2.149

[17] M. M. Hanna, D. A. Steyn-Ross, M. Steyn-Ross, Estimating biomass for New Zealand pasture using optical remote sensing techniques, Geocarto International 14 (3) (1999) 89–94. doi:10.1080/10106049908542121.
URL http://www.tandfonline.com/doi/abs/10.1080/10106049908542121

[18] D. Bella, R. Faivre, F. Ruget, B. Seguin, M. Guérif, B. Combal,

M. Weiss, C. Rebella, Remote sensing capabilities to estimate pasture production in France, International Journal of Remote Sensing 25 (23) (2004) 5359–5372. doi:10.1080/01431160410001719849.
URL https://www.tandfonline.com/doi/full/10.1080/01431160410001719849

[19] Y. Zhou, L. Zhang, J. Xiao, S. Chen, T. Kato, G. Zhou, A Comparison of Satellite-Derived Vegetation Indices for Approximating Gross Primary Productivity of Grasslands, Rangeland Ecology & Management 67 (1) (2014) 9–18. doi:10.2111/REM-D-13-00059.1.
URL https://linkinghub.elsevier.com/retrieve/pii/S1550742414500103

[20] A. C. Amies, J. R. Dymond, J. D. Shepherd, D. Pairman, C. Hoogendoorn, M. Sabetizade, S. E. Belliss, National mapping of New Zealand pasture productivity using temporal Sentinel-2 data, Remote Sensing 13 (8) (2021) 1481. doi:10.3390/rs13081481.
URL https://www.mdpi.com/2072-4292/13/8/1481

[21] M. Boschetti, S. Bocchi, P. A. Brivio, Assessment of pasture production in the Italian Alps using spectrometric and remote sensing information, Agriculture, Ecosystems & Environment 118 (1-4) (2007) 267–272. doi:10.1016/j.agee.2006.05.024.
URL https://linkinghub.elsevier.com/retrieve/pii/S0167880906001770

[22] K. Hogrefe, V. Patil, D. Ruthrauff, B. Meixell, M. Budde, J. Hupp, D. Ward, Normalized Difference Vegetation Index as an Estimator for

Abundance and Quality of Avian Herbivore Forage in Arctic Alaska, Remote Sensing 9 (12) (2017) 1234. doi:10.3390/rs9121234.
URL http://www.mdpi.com/2072-4292/9/12/1234

[23] M. Guerini Filho, T. M. Kuplich, F. L. F. D. Quadros, Estimating natural grassland biomass by vegetation indices using Sentinel 2 remote sensing data, International Journal of Remote Sensing 41 (8) (2020) 2861–2876. doi:10.1080/01431161.2019.1697004.
URL https://www.tandfonline.com/doi/full/10.1080/01431161.2019.1697004

[24] R. Pullanagari, G. Kereszturi, I. Yule, Integrating airborne hyperspectral, topographic, and soil data for estimating pasture quality using recursive feature elimination with random forest regression, Remote Sensing 10 (7) (2018) 1117. doi:10.3390/rs10071117.
URL http://www.mdpi.com/2072-4292/10/7/1117

[25] J. Serrano, S. Shahidian, J. Marques Da Silva, Monitoring seasonal pasture quality degradation in the mediterranean Montado ecosystem: Proximal versus remote sensing, Water 10 (10) (2018) 1422. doi:10.3390/w10101422.
URL http://www.mdpi.com/2073-4441/10/10/1422

[26] Y. Jin, X. Yang, J. Qiu, J. Li, T. Gao, Q. Wu, F. Zhao, H. Ma, H. Yu, B. Xu, Remote sensing-based biomass estimation and its spatio-temporal variations in temperate grassland, Northern China, Remote Sensing 6 (2) (2014) 1496–1513. doi:10.3390/rs6021496.
URL http://www.mdpi.com/2072-4292/6/2/1496

[27] Y. Tang, R. Chen, J. Xie, D. Ma, C. Wang, C. Wang, Q. Xie, G. Yin, Spatiotemporal variations of leaf senescence velocity on the Tibetan Plateau grasslands, Ecological Indicators 156 (2023) 111094. doi:10.1016/j.ecolind.2023.111094.
URL https://linkinghub.elsevier.com/retrieve/pii/S1470160X23012360

[28] A. Colpaert, J. Kumpula, M. Nieminen, Reindeer pasture biomass assessment using satellite remote sensing, ARCTIC 56 (2) (2003) 147–158. doi:10.14430/arctic610.
URL https://journalhosting.ucalgary.ca/index.php/arctic/article/view/63669

[29] D. Alves Aguiar, M. Adami, W. Fernando Silva, B. Friedrich Theodor Rudorff, M. Pupin Mello, J. Dos Santos Vila Da Silva, Modis time series to assess pasture land, in: 2010 IEEE International Geoscience and Remote Sensing Symposium, IEEE, Honolulu, HI, USA, 2010, pp. 2123–2126. doi:10.1109/IGARSS.2010.5649388.
URL http://ieeexplore.ieee.org/document/5649388/

[30] S. Wang, E. Dai, L. Jia, Y. Wang, A. Huang, L. Liao, L. Cai, D. Fan, Assessment of multiple factors and interactions affecting grassland degradation on the Tibetan Plateau, Ecological Indicators 154 (2023) 110509. doi:10.1016/j.ecolind.2023.110509.
URL https://linkinghub.elsevier.com/retrieve/pii/S1470160X23006519

[31] J. B. Lal, A. K. Gulati, M. S. Bist, Satellite mapping of alpine pastures

in the Himalayas, International Journal of Remote Sensing 12 (3) (1991) 435–443. doi:10.1080/01431169108929664.
URL https://www.tandfonline.com/doi/full/10.1080/01431169108929664

[32] F. Stumpf, M. K. Schneider, A. Keller, A. Mayr, T. Rentschler, R. G. Meuli, M. Schaepman, F. Liebisch, Spatial monitoring of grassland management using multi-temporal satellite imagery, Ecological Indicators 113 (2020) 106201. doi:10.1016/j.ecolind.2020.106201.
URL https://linkinghub.elsevier.com/retrieve/pii/S1470160X20301382

[33] D. Weber, M. Schwieder, L. Ritter, T. Koch, A. Psomas, N. Huber, C. Ginzler, S. Boch, Grassland-use intensity maps for Switzerland based on satellite time series: Challenges and opportunities for ecological applications, Remote Sensing in Ecology and Conservation (2023) rse2.372doi:10.1002/rse2.372.
URL https://zslpublications.onlinelibrary.wiley.com/doi/10.1002/rse2.372

[34] D. Weber, G. Schaepman-Strub, K. Ecker, Predicting habitat quality of protected dry grasslands using Landsat NDVI phenology, Ecological Indicators 91 (2018) 447–460. doi:10.1016/j.ecolind.2018.03.081.
URL https://linkinghub.elsevier.com/retrieve/pii/S1470160X1830236X

[35] G. Filippa, E. Cremonese, M. Galvagno, A. Bayle, P. Choler, M. Bassignana, A. Piccot, L. Poggio, L. Oddi, S. Gascoin, S. Costafreda-Aumedes,

G. Argenti, C. Dibari, On the distribution and productivity of mountain grasslands in the Gran Paradiso National Park, NW Italy: A remote sensing approach, International Journal of Applied Earth Observation and Geoinformation 108 (2022) 102718. doi:10.1016/j.jag.2022.102718.
URL https://linkinghub.elsevier.com/retrieve/pii/S0303243422000447

[36] N. Huber, C. Ginzler, R. Pazur, P. Descombes, A. Baltensweiler, K. Ecker, E. Meier, B. Price, Countrywide classification of permanent grassland habitats at high spatial resolution, Remote Sensing in Ecology and Conservation 9 (1) (2023) 133–151. doi:10.1002/rse2.298.
URL https://zslpublications.onlinelibrary.wiley.com/doi/10.1002/rse2.298

[37] Y. Feng, J. Wu, J. Zhang, X. Zhang, C. Song, Identifying the relative contributions of climate and grazing to both direction and magnitude of alpine grassland productivity dynamics from 1993 to 2011 on the northern Tibetan Plateau, Remote Sensing 9 (2) (2017) 136. doi:10.3390/rs9020136.
URL http://www.mdpi.com/2072-4292/9/2/136

[38] L. W. Lass, T. S. Prather, N. F. Glenn, K. T. Weber, J. T. Mundt, J. Pettingill, A review of remote sensing of invasive weeds and example of the early detection of spotted knapweed (Centaurea Maculosa) and babysbreath (Gypsophila Paniculata) with a hyperspectral sensor, Weed Science 53 (2) (2005) 242–251. doi:10.1614/WS-04-044R2.

URL https://www.cambridge.org/core/product/identifier/S0043174500022748/type/journal_article

[39] V. Braunisch, P. Patthey, R. Arlettaz, Where to combat shrub encroachment in alpine timberline ecosystems: Combining remotely-sensed vegetation information with species habitat modelling, Plos One 11 (10) (2016) e0164318. doi:10.1371/journal.pone.0164318.
URL https://dx.plos.org/10.1371/journal.pone.0164318

[40] W. Dietl, P. Berger, M. Ofner, Die Kartierung des Pflanzenstandortes und der futterbaulichen Nutzungseignung von Naturwiesen, Eidg, Forschungsanstalt für landwirtschaftlichen Pflanzenbau und Arbeitsgemeinschaft zur Förderung des Futterbaues, Zürich-Reckenholz, Switzerland (1981).

[41] L. V. Graf, G. Perich, H. Aasen, Eodal: An open-source python package for large-scale agroecological research using earth observation and gridded environmental data, Computers and Electronics in Agriculture 203 (2022) 107487. doi:10.1016/j.compag.2022.107487.
URL https://linkinghub.elsevier.com/retrieve/pii/S0168169922007955

[42] F. N. Fritsch, J. Butland, A method for constructing local monotone piecewise cubic interpolants, SIAM Journal on Scientific and Statistical Computing 5 (2) (1984) 300–304. doi:10.1137/0905021.
URL https://epubs.siam.org/doi/10.1137/0905021

[43] A. Bayle, B. Z. Carlson, V. Thierion, M. Isenmann, P. Choler, Improved

mapping of mountain shrublands using the Sentinel-2 red-edge band, Remote Sensing 11 (23) (2019) 2807. doi:10.3390/rs11232807.
URL https://www.mdpi.com/2072-4292/11/23/2807

[44] G. Filippa, E. Cremonese, M. Galvagno, M. Isabellon, A. Bayle, P. Choler, B. Z. Carlson, S. Gabellani, U. Morra di Cella, M. Migliavacca, Climatic drivers of greening trends in the Alps, Remote Sensing 11 (21) (2019) 2527. doi:10.3390/rs11212527.
URL https://www.mdpi.com/2072-4292/11/21/2527

[45] J. Yan, G. Zhang, H. Ling, F. Han, Comparison of time-integrated NDVI and annual maximum NDVI for assessing grassland dynamics, Ecological Indicators 136 (2022) 108611. doi:10.1016/j.ecolind.2022.108611.
URL https://linkinghub.elsevier.com/retrieve/pii/S1470160X22000826

[46] M. K. Schneider, R. Law, J. B. Illian, Quantification of neighbourhood-dependent plant growth by bayesian hierarchical modelling, Journal of Ecology 94 (2) (2006) 310–321. doi:10.1111/j.1365-2745.2005.01079.x.
URL https://besjournals.onlinelibrary.wiley.com/doi/10.1111/j.1365-2745.2005.01079.x

[47] Student, Probable error of a correlation coefficient, Biometrika 6 (2-3) (1908) 302–310. doi:10.1093/biomet/6.2-3.302.
URL https://doi.org/10.1093/biomet/6.2-3.302

[48] T. Kattenborn, F. E. Fassnacht, S. Schmidtlein, Differentiating plant functional types using reflectance: Which traits make the difference?, Remote Sensing in Ecology and Conservation 5 (1) (2019) 5–19. doi:10.1002/rse2.86.
URL https://zslpublications.onlinelibrary.wiley.com/doi/10.1002/rse2.86

[49] F. J. Swanson, T. K. Kratz, N. Caine, R. G. Woodmansee, Landform effects on ecosystem patterns and processes, BioScience 38 (2) (1988) 92–98. doi:10.2307/1310614.
URL https://academic.oup.com/bioscience/article-lookup/doi/10.2307/1310614

[50] T. Jonas, C. Rixen, M. Sturm, V. Stoeckli, How alpine plant growth is linked to snow cover and climate variability, Journal of Geophysical Research: Biogeosciences 113 (G3) (2008). doi:10.1029/2007JG000680.
URL https://onlinelibrary.wiley.com/doi/abs/10.1029/2007JG000680

[51] L. L. Tieszen, W. D. Billings, F. Golley, O. L. Lange, J. S. Olson (Eds.), Vegetation and Production Ecology of an Alaskan Arctic Tundra, Vol. 29 of Ecological Studies, Springer New York, New York, NY, 1978. doi:10.1007/978-1-4612-6307-4.
URL http://link.springer.com/10.1007/978-1-4612-6307-4

[52] N. Fetcher, G. R. Shaver, Environmental sensitivity of ecotypes as a potential influence on primary productivity, The American Naturalist

136 (1) (1990) 126–131. doi:10.1086/285085.
URL https://www.journals.uchicago.edu/doi/10.1086/285085

[53] M. D. Walker, P. J. Webber, E. H. Arnold, D. Ebert-May, Effects of interannual climate variation on aboveground phytomass in alpine vegetation, Ecology 75 (2) (1994) 393–408. doi:10.2307/1939543.
URL https://onlinelibrary.wiley.com/doi/abs/10.2307/1939543

[54] T. C. Parker, S. L. Unger, M. L. Moody, J. Tang, N. Fetcher, Intraspecific variation in phenology offers resilience to climate change for *Eriophorum Vaginatum*, Arctic Science 8 (3) (2022) 935–951. doi:10.1139/as-2020-0039.
URL https://cdnsciencepub.com/doi/10.1139/as-2020-0039

[55] P. Choler, Growth response of temperate mountain grasslands to interannual variations in snow cover duration, Biogeosciences 12 (12) (2015) 3885–3897. doi:10.5194/bg-12-3885-2015.
URL https://bg.copernicus.org/articles/12/3885/2015/

[56] J. Xie, M. Kneubühler, I. Garonna, C. Notarnicola, L. De Gregorio, R. De Jong, B. Chimani, M. E. Schaepman, Altitude-dependent influence of snow cover on alpine land surface phenology, Journal of Geophysical Research: Biogeosciences 122 (5) (2017) 1107–1122. doi:10.1002/2016JG003728.
URL https://agupubs.onlinelibrary.wiley.com/doi/10.1002/2016JG003728

[57] C. Körner, The cold range limit of trees, Trends in Ecology & Evolution 36 (11) (2021) 979–989. doi:10.1016/j.tree.2021.06.011. URL https://linkinghub.elsevier.com/retrieve/pii/S0169534721001841

Monitoring the response of mountain pastures habitats to climate variability using satellite remote sensing

Fabio Oriani, Helge Aasen, Manuel Schneider

Supplemental material 1 - annual NDVI and RSD graphs for all examined years (displayed in couples)

NDVI (dashed lines and envelopes)
RSD (continuous lines)
For NDVI, the evenlope is delimited by the the 25-th and 75-th percentile of the pixel-value distribution, while the dashed line represents the median.

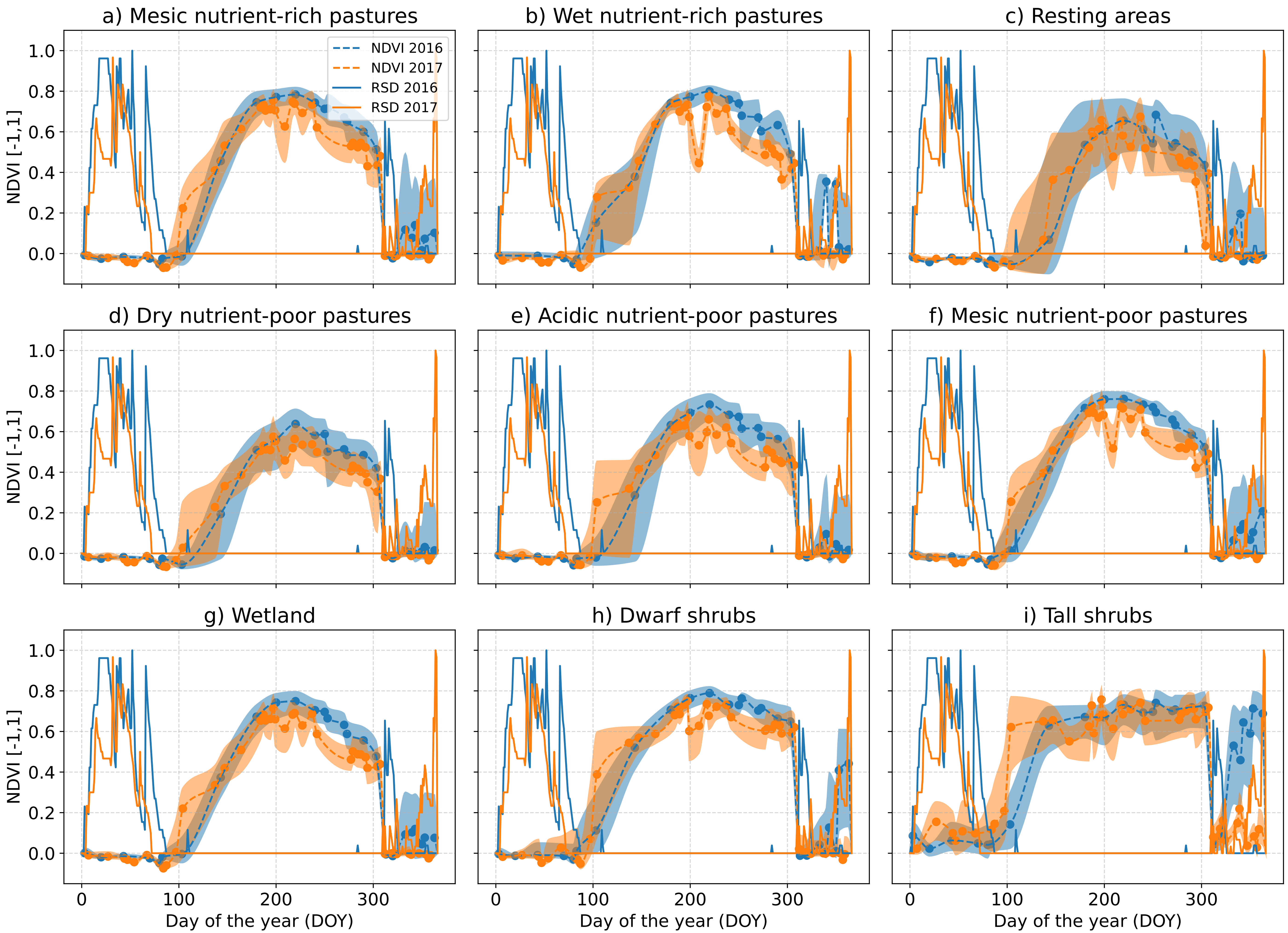
a) Mesic nutrient-rich pastures
b) Wet nutrient-rich pastures
c) Resting areas
d) Dry nutrient-poor pastures
e) Acidic nutrient-poor pastures
f) Mesic nutrient-poor pastures
g) Wetland
h) Dwarf shrubs
i) Tall shrubs
NDVI 2016
NDVI 2017
RSD 2016
RSD 2017
NDVI [-1,1]
Day of the year (DOY)
0
100
200
300
0.0
0.2
0.4
0.6
0.8
1.0

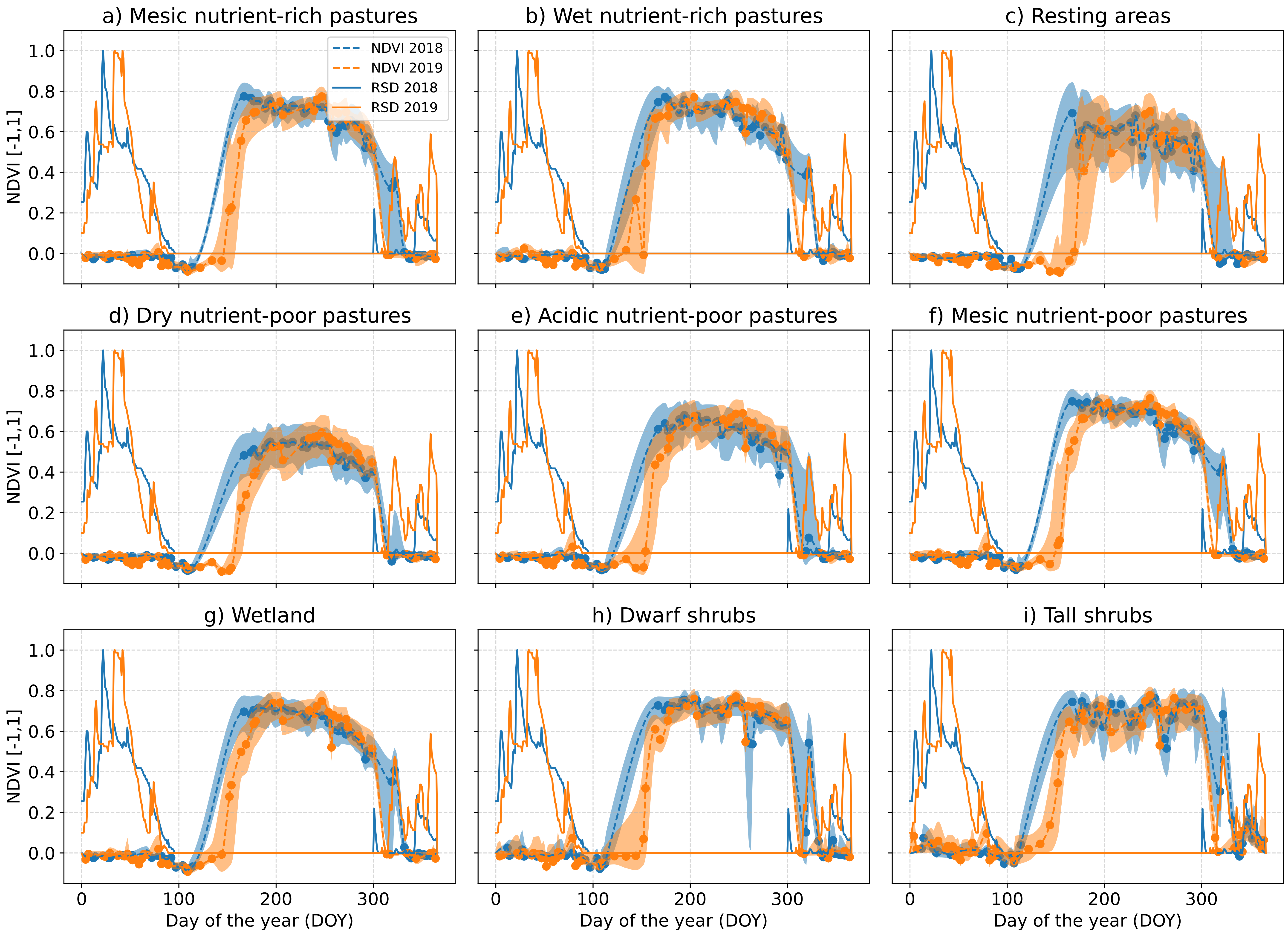
a) Mesic nutrient-rich pastures
b) Wet nutrient-rich pastures
c) Resting areas
d) Dry nutrient-poor pastures
e) Acidic nutrient-poor pastures
f) Mesic nutrient-poor pastures
g) Wetland
h) Dwarf shrubs
i) Tall shrubs
NDVI 2018
NDVI 2019
RSD 2018
RSD 2019
NDVI [-1,1]
Day of the year (DOY)
0.0
0.2
0.4
0.6
0.8
1.0
0
100
200
300

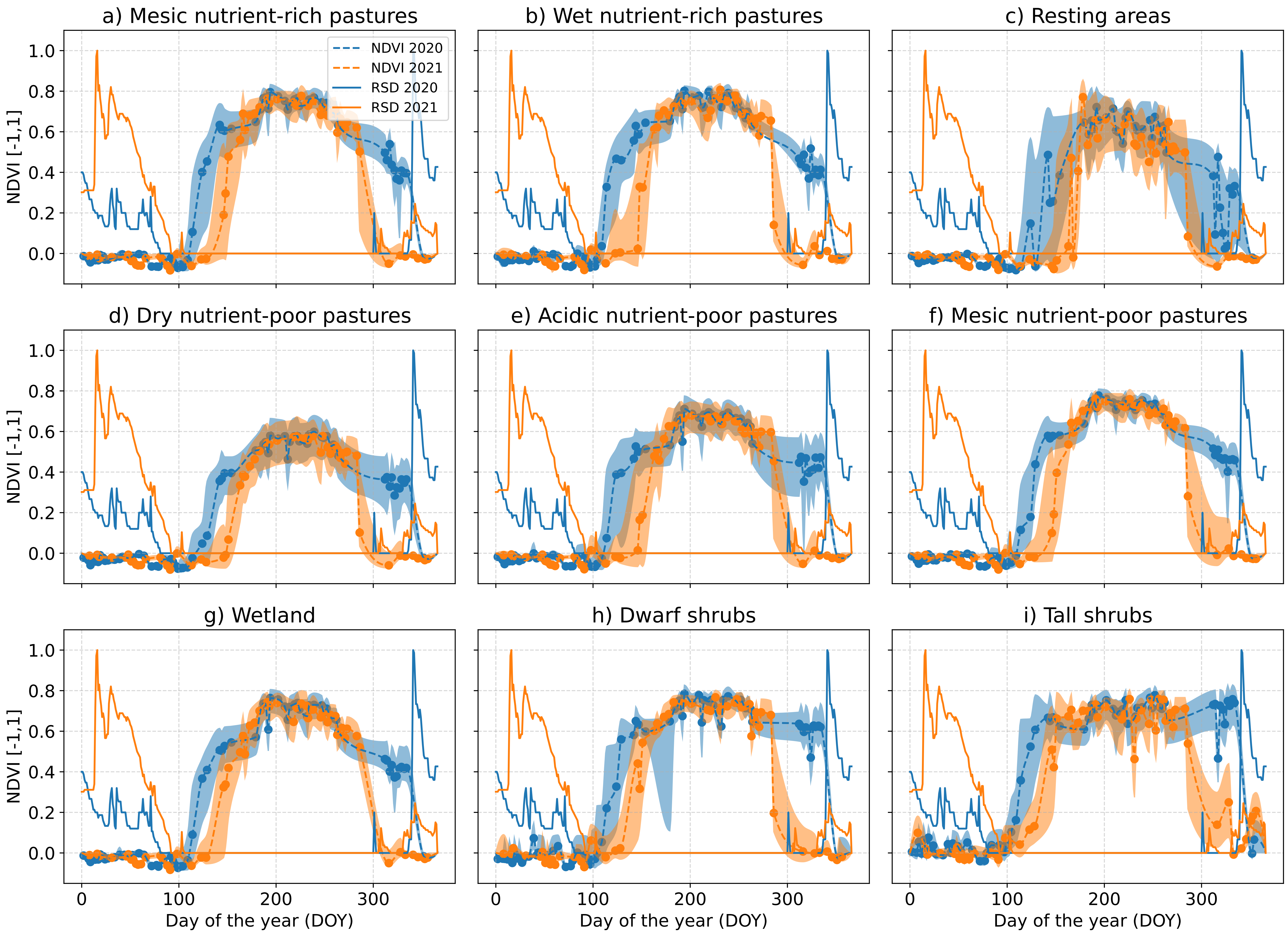

a) Mesic nutrient-rich pastures
b) Wet nutrient-rich pastures
c) Resting areas
d) Dry nutrient-poor pastures
e) Acidic nutrient-poor pastures
f) Mesic nutrient-poor pastures
g) Wetland
h) Dwarf shrubs
i) Tall shrubs
NDVI 2020
NDVI 2021
RSD 2020
RSD 2021
NDVI [-1,1]
Day of the year (DOY)
0.0
0.2
0.4
0.6
0.8
1.0
0
100
200
300

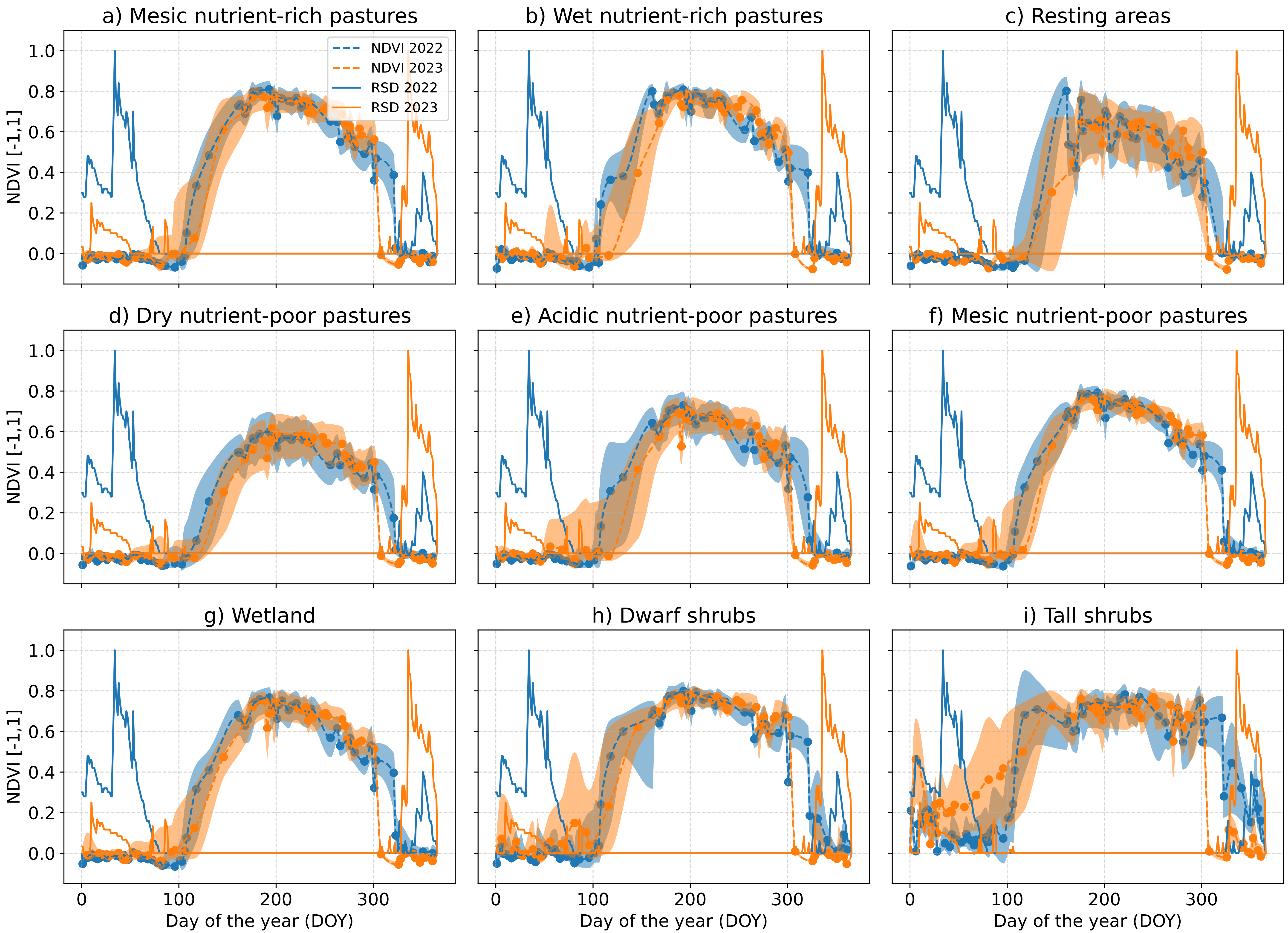

a) Mesic nutrient-rich pastures
b) Wet nutrient-rich pastures
c) Resting areas
d) Dry nutrient-poor pastures
e) Acidic nutrient-poor pastures
f) Mesic nutrient-poor pastures
g) Wetland
h) Dwarf shrubs
i) Tall shrubs
NDVI 2022
NDVI 2023
RSD 2022
RSD 2023
NDVI [-1,1]
Day of the year (DOY)
0.0
0.2
0.4
0.6
0.8
1.0
0
100
200
300